



Article

Study of Influence of Width to Thickness Ratio in Sheet Metals on Bendability under Ambient and Superimposed Hydrostatic Pressure

Mohammadmehdi Shahzamanian ^{1,2,*} , David Lloyd ³, Amir Partovi ¹ and Peidong Wu ¹

¹ Department of Mechanical Engineering, McMaster University, Hamilton, ON L8S 4L7, Canada; partovia@mcmaster.ca (A.P.); peidong@mcmaster.ca (P.W.)

² Department of Civil and Environmental Engineering, University of Alberta, Edmonton, AB T6G 2W2, Canada

³ Aluminum Materials Consultants, 106 Nicholsons Road, Bath, ON K0H 1G0, Canada; almatcon@gmail.com

* Correspondence: mmshahzamanian@gmail.com or mshahzam@ualberta.ca

Abstract: The effect of the width to thickness ratio on the bendability of sheet metal is investigated using the finite element method (FEM) employing the Gurson–Tvergaard–Needleman (GTN) model. Strain path changes in the sheet with change in the width/thickness ratio. It is shown that bendability and fracture strain increase significantly by decrease in the width/thickness ratio. The stress state is almost uniaxial when the stress ratio (α) is close to zero for narrow sheets. Stress ratio is nothing but the major stress to minor stress ratio. This delays the growth and coalescence of micro-voids as the volumetric strain and stress triaxiality (pressure/effective stress) decrease. On the other hand, ductility decreases with increase in α for wider sheets. Fracture bending strain is calculated and, as expected, it increases with decrease in the width/thickness ratio. Furthermore, a brief study is performed to understand the effect of superimposed hydrostatic pressure on fracture strain for various sheet metals with different width/thickness ratios. It is found that the superimposed hydrostatic pressure increases the ductility, and that the effect of the width/thickness ratio in metals on ductility is as significant as the effect of superimposed hydrostatic pressure. Numerical results are found to be in good agreement with experimental observations.

Keywords: bendability; fracture; width to thickness ratio; finite element method (FEM)



Citation: Shahzamanian, M.; Lloyd, D.; Partovi, A.; Wu, P. Study of Influence of Width to Thickness Ratio in Sheet Metals on Bendability under Ambient and Superimposed Hydrostatic Pressure. *Appl. Mech.* **2021**, *2*, 542–558. <https://doi.org/10.3390/applmech2030030>

Received: 29 June 2021

Accepted: 26 July 2021

Published: 30 July 2021

Publisher's Note: MDPI stays neutral with regard to jurisdictional claims in published maps and institutional affiliations.



Copyright: © 2021 by the authors. Licensee MDPI, Basel, Switzerland. This article is an open access article distributed under the terms and conditions of the Creative Commons Attribution (CC BY) license (<https://creativecommons.org/licenses/by/4.0/>).

1. Introduction

Bending is an important property in sheet metals as bending occurs as a part of several forming operations, such as in deep drawing in auto industry [1–4]. In [5–7], the bending properties of various materials have been studied, and in [8,9] bending performance was studied using the three-point bend test. On the other hand, there exist several methods to enhance the ductility of sheet metals under bending, such as superimposing hydrostatic pressure [10], cladding [11] and reducing the width/thickness of metals [12]. The strain state in sheet metals changes with changing the width/thickness of a specimen and the fracture strain increases with decreasing this ratio. However, to the best of our knowledge, the effect of width/thickness of a specimen on bendability is not considered numerically in detail elsewhere.

It is explained in [1,2] that bendability of sheet metals is dependent on the width to thickness ratio of sheet metals. In fact, the fracture strain in metals is dependent on stress triaxiality [13,14]. Figure 1 shows the dependency of fracture strain on stress triaxiality for a typical steel material. It is observed that the fracture strain increases from plain strain state to the uniaxial state when the stress triaxiality decreases. The uniaxial and plain strain state are marked with arrows. The stress state of a material changes with changing the width to thickness ratio. For narrow sheets, the stress state is almost uniaxial when stress ratio (α) is close to zero and the ductility decreases with increase in α for wider sheets. The maximum achievable α is 0.5 for the plane strain state where the ductility is a minimum.

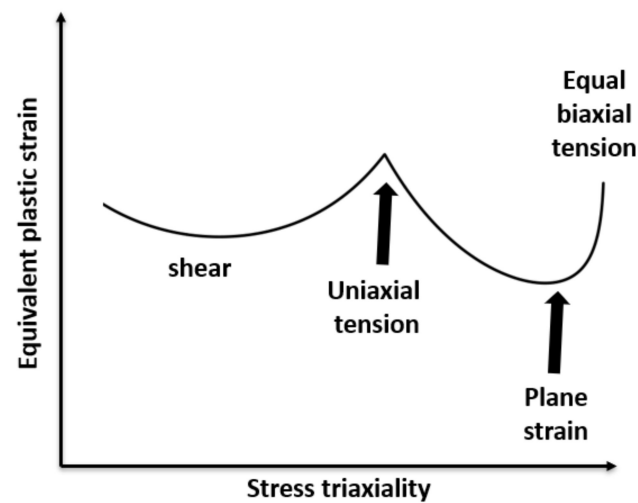


Figure 1. Dependency of fracture strain on stress triaxiality under various stress states for a typical steel material.

It is observed in [15] through quantitative metallography and fractography that a significant increase in ductility happens with the suppression of micro-void development. Overall, it is generally accepted that a superimposed hydrostatic pressure increases ductility as it delays or completely eliminates the void growth and nucleation [12,16–21]. Kao et al. [12] presented the forming limit diagrams (surface tensile strain vs. compressive strain at fracture) for sheets under various hydrostatic pressures, and it was found that fracture under bending increased with increase in hydrostatic pressure and caused the forming limit diagram to increase, which was attributed to suppression of void growth. However, the ductility enhancement in [12] for sheet metals under hydrostatic pressure to reach the fracture point required excessive deformation which was beyond the testing capacity of their available equipment. Therefore, they used a different approach in which rectangular specimens with various width/thickness ratios were tested under bending and three different levels of hydrostatic pressure. They investigated the effect of superimposed hydrostatic pressure on the workability and ductility of 1045 spheroidized steel in three-point bending with various width/thickness ratios. The Gurson-Tvergaard-Needleman (GTN) model [22–24] considers the effect of micro-voids that limit the formability of sheet metals. The GTN model as an improvement of the original Gurson model [25] considers void nucleation and coalescence that lead to fracture. The effect of pre-strain on bendability has been studied by Shahzamanian et al. [26] using the GTN model and it was observed that the pre-strain decreases the fracture strain in sheet metals under bending. Schowtjak et al. [27] used a machine learning approach to predict the void volume fraction in the GTN model for sheet metals under bending. Anderson et al. [28] used the GTN model to study and compare the ductility in sheet metals under plain strain bending and far-field plain strain tension. It was shown by Anderson et al. [28] that ductility in sheet metals under bending is higher than that under plain strain tension. Achineethongkham and Uthaisangsuk [29] analyzed the forming behavior of high strength steels using the GTN model. Additionally, the GTN model has been extended suitably for anisotropic materials, and the results were verified and used for a typical aluminum alloy in [30]. It is to be noted that the conventional GTN model is not dependent on stress state [31], and void growth under compression is not considered in this model [10–37]. Although the GTN model has these limitations, overall the GTN model has been used frequently to simulate the deformation process including fracture for different materials and in various applications [32–36].

The effect of superimposed hydrostatic pressure on the bendability of sheet metals using the GTN model in ABAQUS is investigated in [10]. In this study, it is discussed how hydrostatic pressure suppresses the void growth leading to increase in ductility.

The pressure and stress triaxiality decrease with an increase in superimposed hydrostatic pressure. Then, the void growth decreases, and it causes the fracture strain to increase. In another study [11], the effect of cladding on the ductility of sheet metals is investigated using the GTN model. A softer material is clad to a base metal with a perfect bonding. The fracture strain of the cladding material is higher than that in the base metal. Consequently, this matter helps increase the ductility in metals. Furthermore, there exists a fracture initiation transition from the interface between the core and base metals to the outer surface of the sheet with increasing the clad thickness percentage. This phenomenon has been successfully shown in [11] as observed in experiments. From [10,11], it is clear that the FEM using the GTN model is a useful and successful approach to perform various analyses and to understand various effects on the ductility of metals in three-point bending tests.

The aim of this study is to perform a numerical study of the effect of the width/thickness ratio on fracture in sheet metal under three-point bending. In fact, it is shown how the width to thickness ratio affects the bendability in sheet metals and we attempted to explain this matter in detail. This effect is explained in a stepwise manner through modeling of various bending tests with different width values. The finite element (FE) modeling is performed to understand the reason for increasing fracture strain with decreasing width in a sheet metal. All the simulations presented in this study are performed using ABAQUS/Explicit [37] based on the GTN model. Additionally, the effect of hydrostatic pressure on the ductility of sheet metals with various widths is discussed. The numerical results are found to be in good agreement with experimental observations in [12].

2. Constitutive Model

The Gurson-Tvergaard-Needleman (GTN) model [22–24] is used in this study, which is on the basis of damage growth in metals due to nucleation, void growth and coalescence; this model was originally developed by Gurson [25]. The void growth is a function of the plastic strain rate \mathbf{D}^P :

$$\left(\dot{f}\right)_{growth} = (1 - f)\mathbf{I} : \mathbf{D}^P \tag{1}$$

and the void nucleation in ABAQUS is assumed to be strain controlled as follows:

$$\dot{f} = \bar{A}\bar{\epsilon}^{\cdot P} \tag{2}$$

where $\bar{\epsilon}^{\cdot P}$ is the effective plastic strain rate, and the parameter \bar{A} is chosen so that nucleation follows a normal distribution, as suggested by Chu and Needleman [38]:

$$\bar{A} = \frac{f_N}{S_N\sqrt{2\pi}} \exp\left[-\frac{1}{2}\left(\frac{\bar{\epsilon}^p - \epsilon_N}{S_N}\right)^2\right] \tag{3}$$

here, ϵ_N is the average void nucleating strain, f_N is the volume fraction of void nucleating particles, and S_N is the standard deviation of void nucleating strain.

The growth of existing voids and the nucleation of new voids are considered in the evolution of void volume fraction as follows:

$$\dot{f} = \left(\dot{f}\right)_{growth} + \left(\dot{f}\right)_{nucleation} \tag{4}$$

and the function of void volume fraction ($f^*(f)$) is defined to consider coalescence as follows:

$$f^* = \begin{cases} f & f \leq f_c \\ f_c + \frac{f_u^* - f_c}{f_f - f_c}(f - f_c) & f > f_c \end{cases} \tag{5}$$

where f_c is the critical void volume fraction when coalescence happens and f_f is the void volume fraction at failure. Lastly, the parameter $f_u^* = \frac{1}{q_1}$ is defined. It should be mentioned

that void growth and nucleation do not happen when the stress state of an element is compressive in ABAQUS, and that void growth and nucleation only happen in tension.

Finally, the approximate yield function to be used in which f^* is distributed randomly is as follows:

$$\Phi(\sigma, \bar{\sigma}, f) = \frac{\sigma_e^2}{\bar{\sigma}^2} + 2f^* q_1 \cosh\left(\frac{3q_2 \sigma_H}{2\bar{\sigma}}\right) - [1.0 + (q_1 f^*)^2] = 0 \tag{6}$$

where σ is the macroscopic Cauchy stress tensor and σ_e , σ_H and $\bar{\sigma}$ are equivalent stress, hydrostatic stress and matrix stress, respectively. Additionally, q_1 and q_2 are calibrated parameters.

The uniaxial elastic–plastic undamaged stress–strain curve for the matrix material is provided by the following power-law form:

$$\bar{\epsilon} = \begin{cases} \frac{\bar{\sigma}}{E} & \bar{\sigma} \leq \sigma_y \\ \frac{\sigma_y}{E} \left(\frac{\bar{\sigma}}{\sigma_y}\right)^n & \bar{\sigma} > \sigma_y \end{cases} \tag{7}$$

3. Problem Formulation and Method of Solution

Simulation of a three-dimensional (3D) bending test, using ABAQUS software, is performed in this study. A schematic presentation of a metal sheet with length L_0 and thickness t is shown in Figure 2. Rigid bodies are considered for both punch and mandrel with radii R_p and R_m , respectively. The mandrel is stationary with a length span of L_m when the punch applies a force in the middle section of the sheet. The sheet rests on the two mandrel and punch motion deforms the sheet.

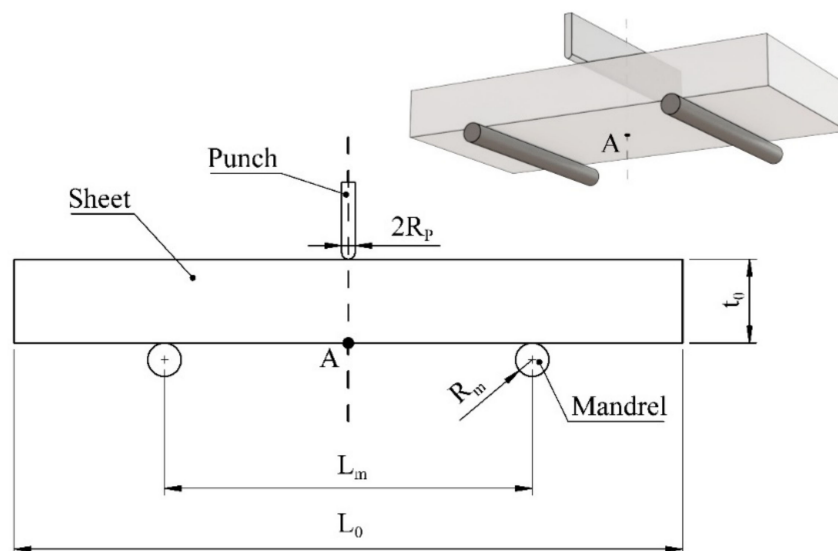


Figure 2. Schematic of three-point bending test.

4. Results and Discussion

These values of mechanical properties are taken from Tvergaard and Needleman [22]; material properties are presented in Table 1. Three-dimensional fully reduced integration element C3D8R in ABAQUS/Explicit is considered and length of sheet (L) and thickness (t_0) are 20 mm and 2.5 mm, respectively. Additionally, R_m , R_p and L_m are 0.25 mm, 0.2 mm and 11 mm, respectively.

Table 1. Material properties for the sheet metal.

	E (GPa)	ν	σ_y (MPa)	n	q_1	q_2	f_N	ϵ_N	S_N	f_c	f_f
Matrix material	71	0.3	234.3	10	1.5	1.0	0.04	0.3	0.1	0.15	0.25

It should be mentioned that although the three-point bending test is a static analysis, ABAQUS/Explicit is used in this study as ABAQUS/Standard is not able to provide the failure in the GTN model. However, a mass scaling method with sufficient low target time increment is used to minimize the dynamic effect of the sample.

The FE configuration of the 3D three-point bending test in ABAQUS is shown in Figure 3. Due to the symmetry, only half of the sheet is investigated. $110 \times 60 \times 12$ C3D8R elements (110 elements in length direction, 60 elements in thickness direction and width elements in Z direction) in ABAQUS/Explicit is used. Mesh sensitivity on prediction of fracture strain in tensile tests simulation using FEM is reported in [38–42]. The effect of mesh sensitivity on the force-displacement curve is shown in Figure 4 for three different meshes. It is found that the size of elements has an insignificant effect on the fracture initiation. Additionally, fracture strains for different meshes are calculated and shown in Table 2. Fracture strain is $\epsilon_c = \ln\left(\frac{t_0}{t_f}\right)$, where t_0 and t_f are the initial and final thickness of sheet in the middle section of specimen, respectively.

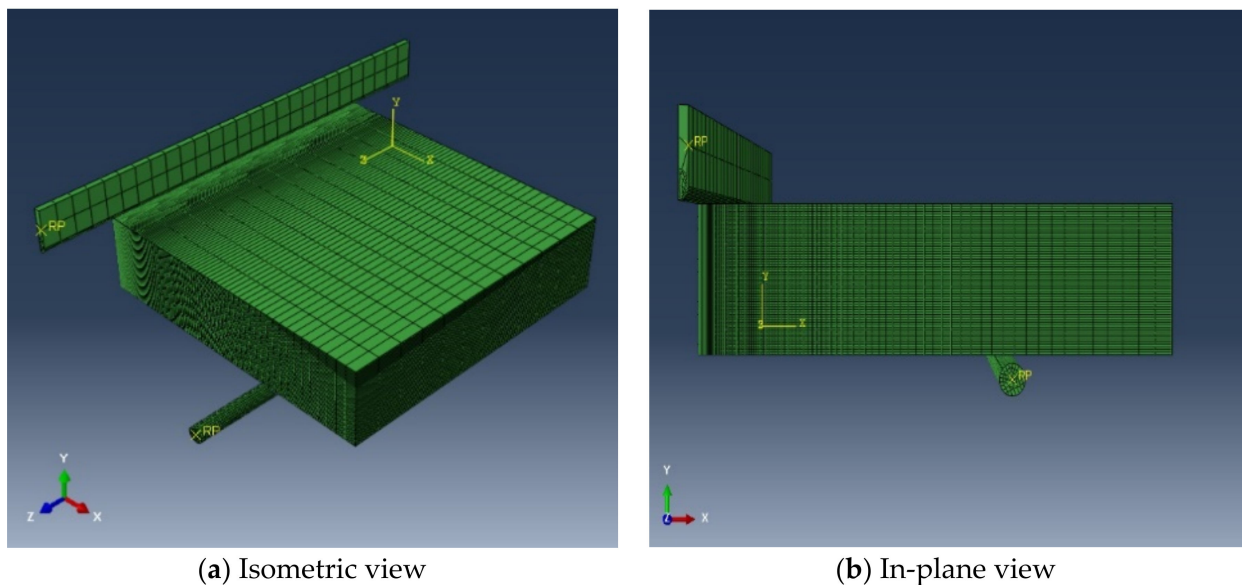


Figure 3. A typical mesh with $110 \times 60 \times 12$ 3D elements (C3D8R in ABAQUS/Explicit).

Table 2. Effect of mesh on fracture strain.

Mesh distribution	$60 \times 110 \times 4$	$60 \times 110 \times 8$	$60 \times 110 \times 12$
Fracture strain	0.279	0.288	0.283

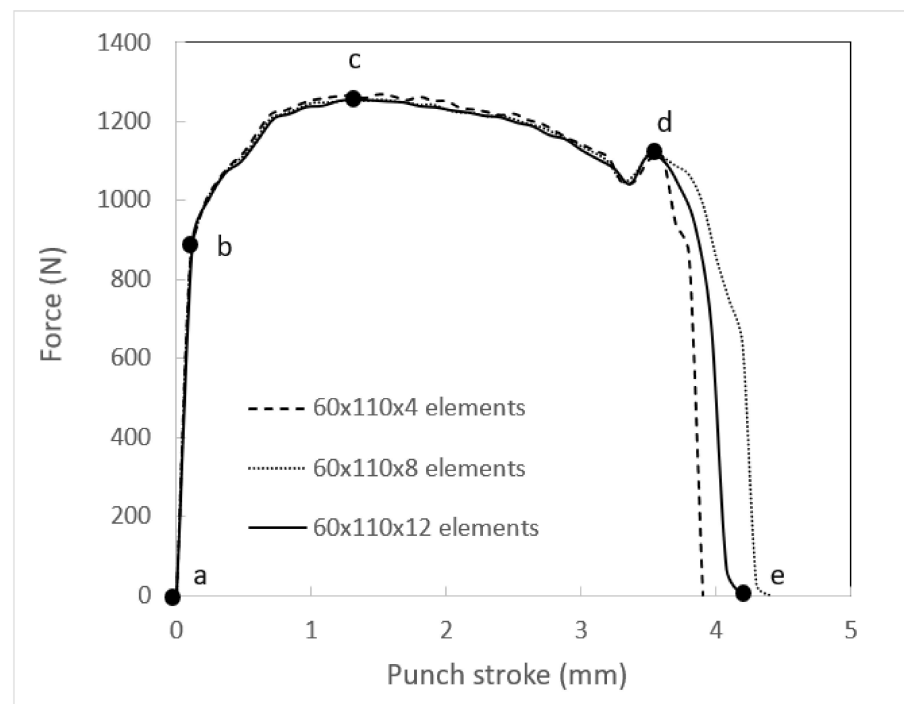


Figure 4. Effect of mesh sensitivity on force-displacement curve.

The deformation steps for a sheet with 10 mm width are shown in Figure 5 step-by-step up to complete fracture. The steps are marked on the force-displacement curve in Figure 4. Force increases linearly up to step “b” when the sheet is in the elastic region. Then, it reaches the maximum value with advancement of punch in step “c”. Fracture initiates in step “d” with further punch advancement, and eventually complete failure in step “e” happens when the load drops and it reaches zero value.

4.1. Effect of Width to Thickness Ratio on Bendability

The effect of specimen width on the force-displacement curve and bendability is shown in Figure 6, while the thickness is constant for all cases. It is found that the force-displacement curve rises with increasing width because the volume of material increases, and it takes more force to bend the specimen. However, the ductility decreases with an increase in width as the stress ratio increases and the stress state changes from uniaxial tensile to in-plane plane strain. Additionally, it must be mentioned that fracture does not happen for the sheet with 2.5 mm width. Later in this section, the strain path for each case will be shown and it will be understood how strain path affects the fracture strain and ductility.

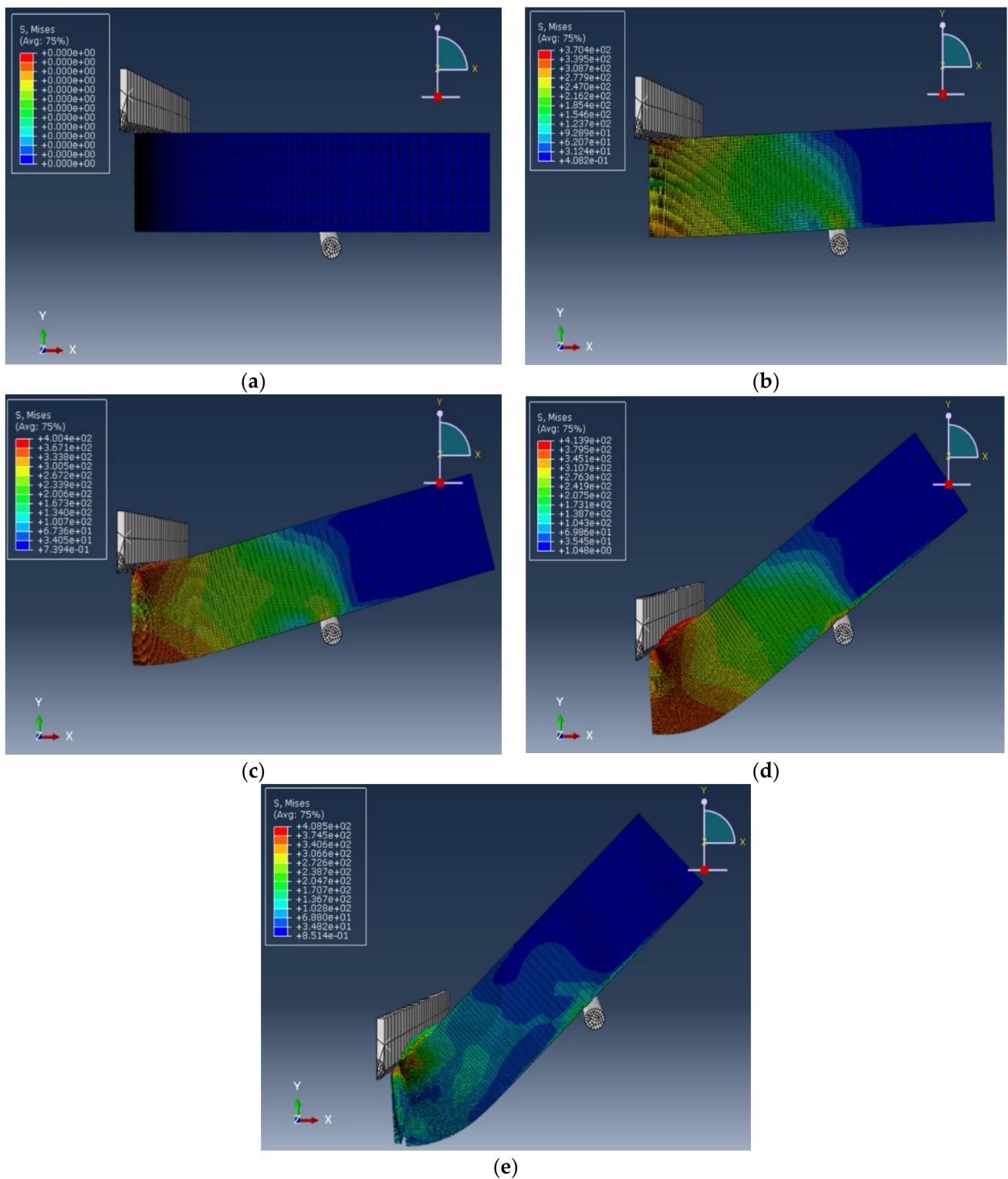


Figure 5. Deformation steps in a sheet metal with 10 mm width under bending (the steps (a–e) are marked on the force-displacement curve in Figure 4).

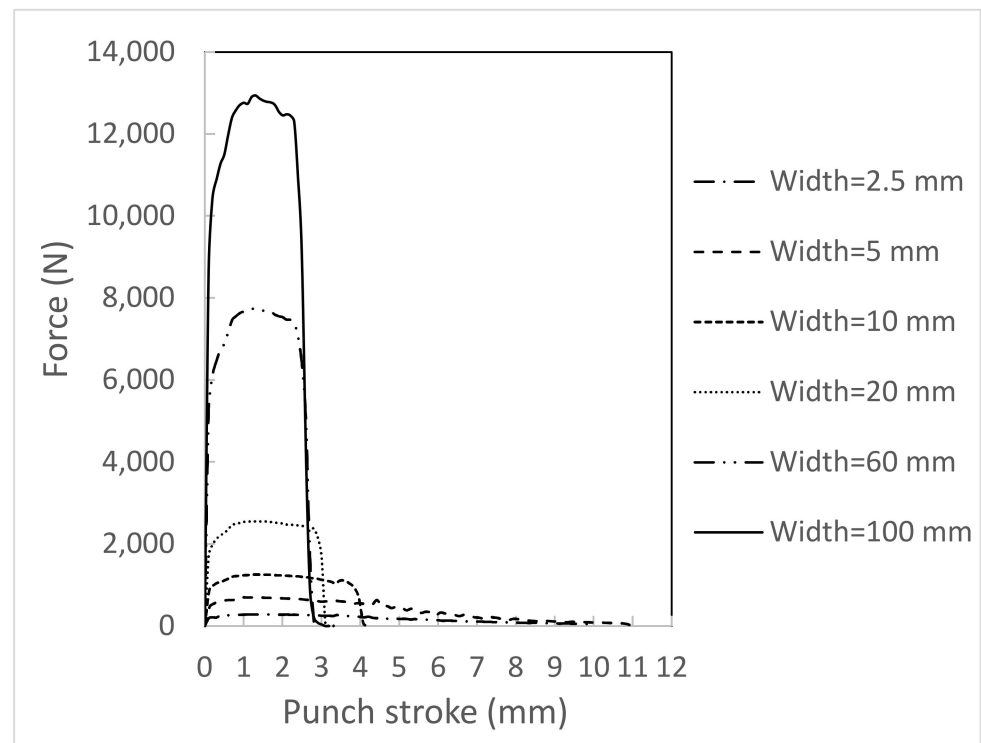


Figure 6. Force-displacement curves in metal sheets with various widths.

The stress ratio at the outer surface in the middle section of a sheet metal changes with change of width/thickness ratio. The strain state accordingly on the outer surface at the middle section of the specimen changes with changing width in sheet metals. For the wide specimen, the stress ratio is close to 0.5 corresponding to in-plane plane strain state, and for a narrow specimen the stress ratio is close to zero corresponding to a uniaxial tensile state [1]. The major and minor strains at point A (see Figure 2) for six different sheets with different widths are shown in Figure 7 with the same thickness value. Here, ϵ_{11} and ϵ_{22} are the major and minor strains, respectively. As shown in Figure 7, minor strain is almost zero for wide sheets and its absolute value starts to increase with decreasing the sheet width. It is clearly shown in Figure 7e,f that the strain ratio for sheets with widths 5 and 2.5 mm reaches a negative value, close to what happens in the uniaxial tension test. Figure 8 shows the volumetric strain ($\epsilon_{11} + \epsilon_{22} + \epsilon_{33}$) at point A for these six cases and it is found that this value decreases with decreasing width/thickness ratio as shown in Figure 8. This helps decrease the void growth following Equation (1) and it leads to higher bendability. It is to be noted that fracture does not occur for the sheet with a width of 2.5 mm; this is why the volumetric strain increases and then decreases when it only slides over the mandrel with less force.

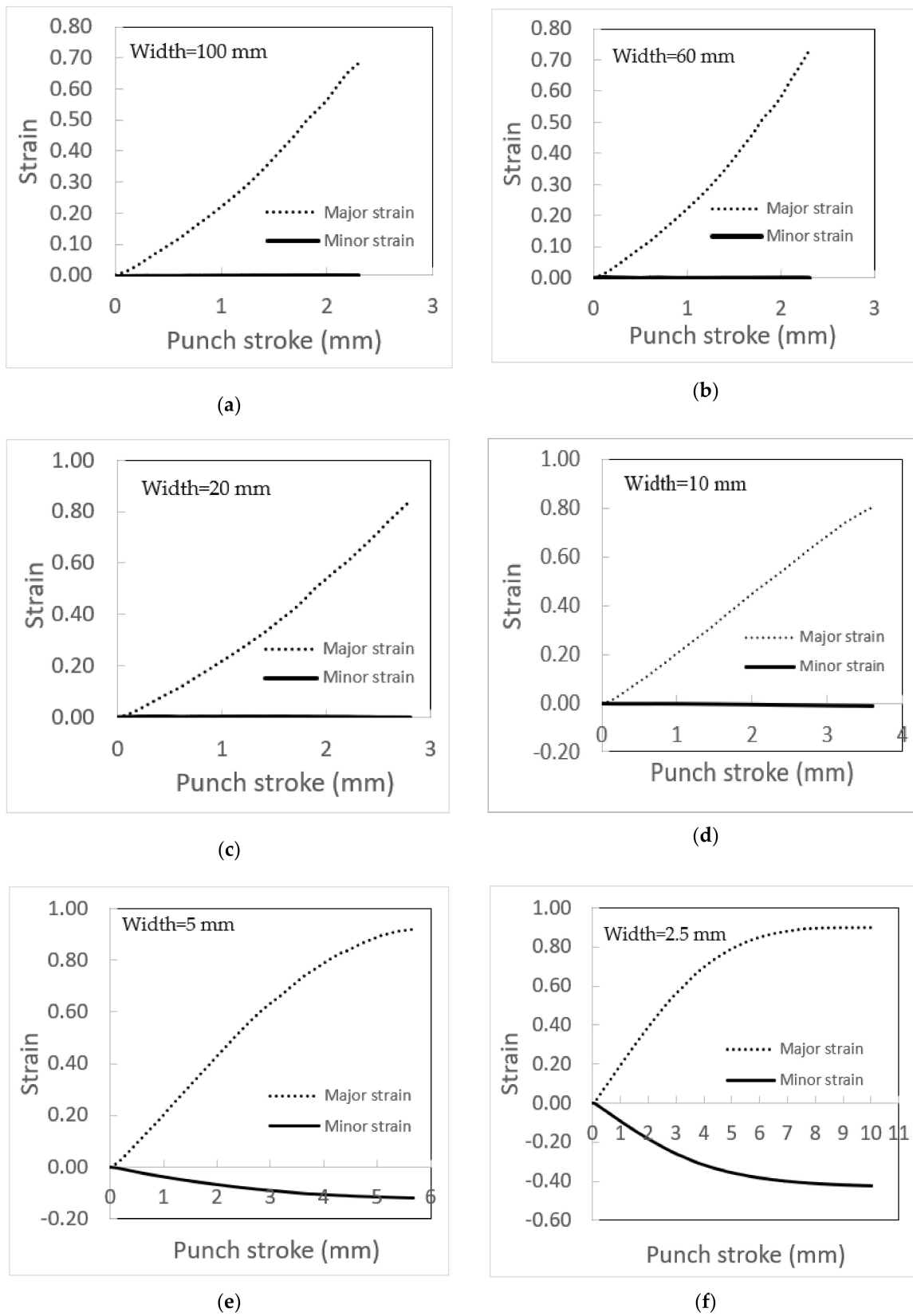


Figure 7. Major and minor strain in metal sheets with various width/thickness ratios; (a) width = 100 mm, (b) width = 60 mm, (c) width = 20 mm, (d) width = 10 mm, (e) width = 5 mm, and (f) width = 2.5 mm.

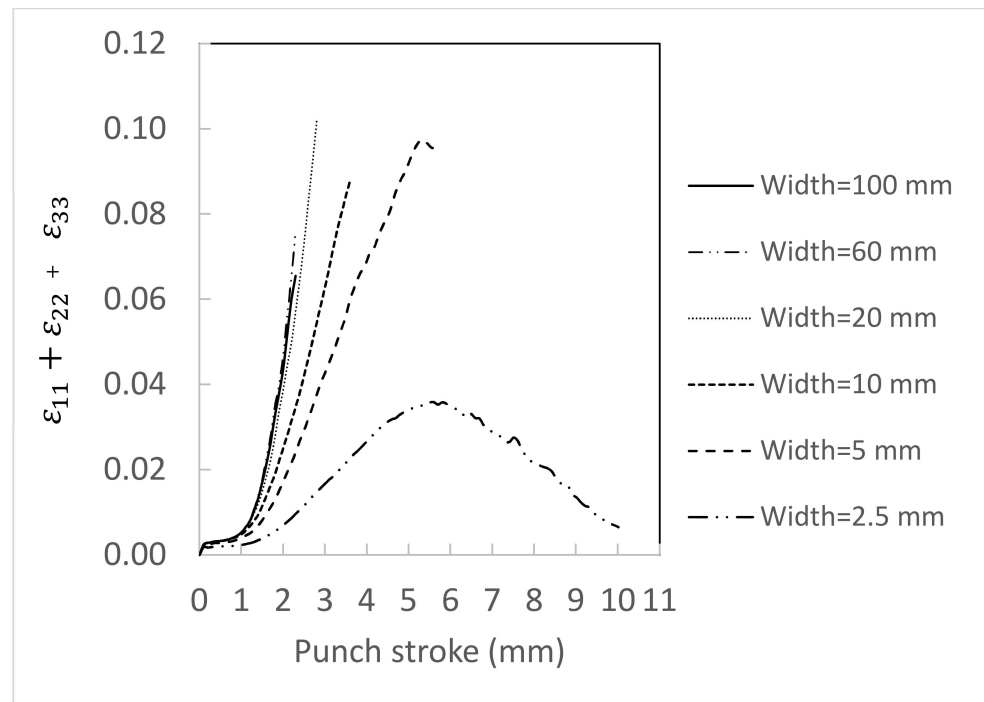
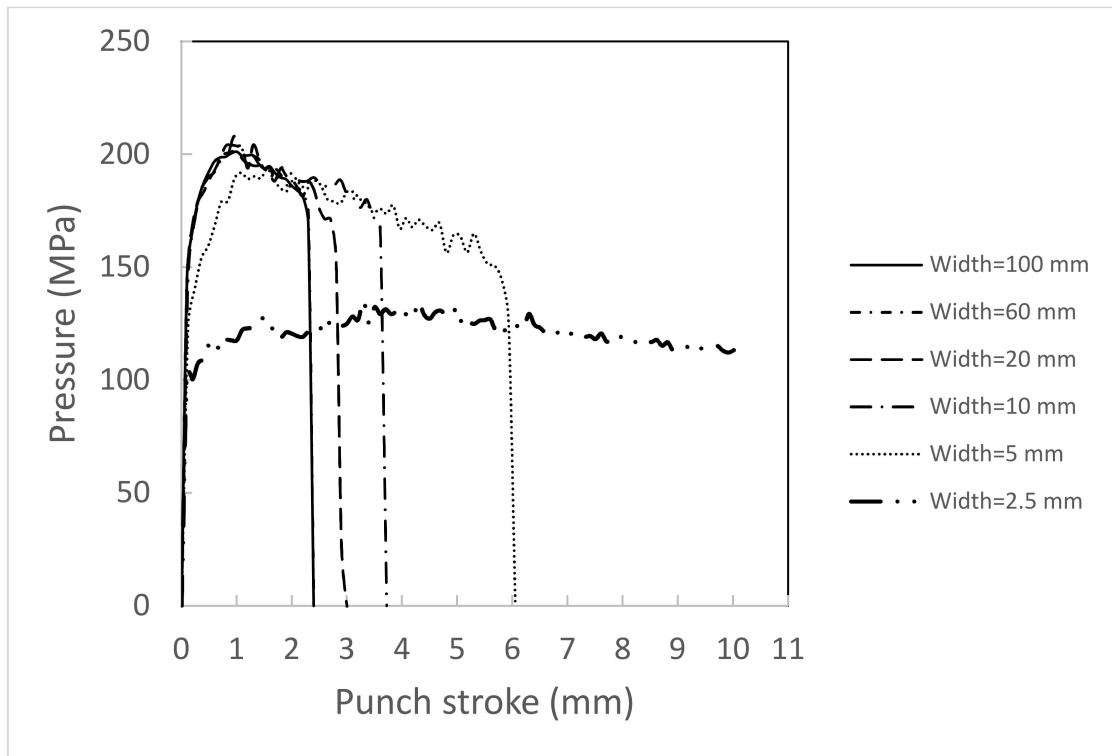


Figure 8. Volumetric strain in metal sheets with various widths.

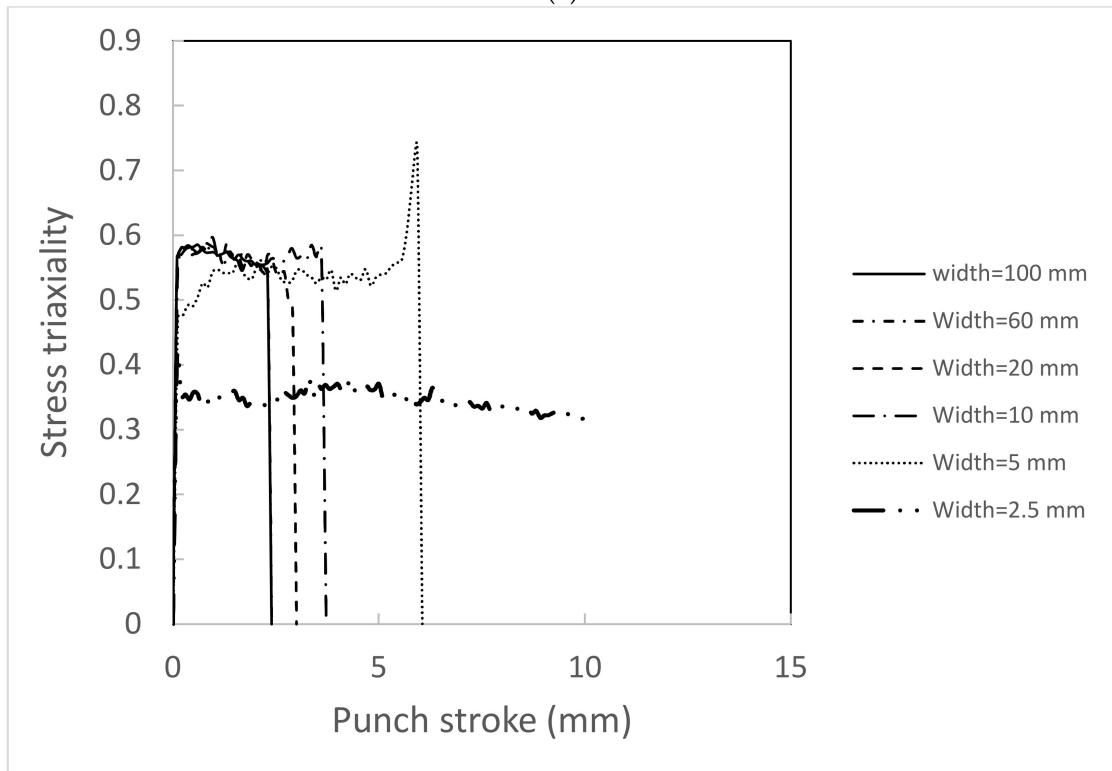
Figure 9 presents the hydrostatic pressure $\sigma_H = (1/3)(\sigma_{xx} + \sigma_{yy} + \sigma_{zz})$ and stress triaxiality $\frac{\sigma_H}{\sigma}$ at point A (see Figure 2), where fracture initiates as a function of punch stroke under various widths. It is found that stress triaxiality and hydrostatic pressure decrease with increased pressure, helping to delay void growth (Equation (6)). Stress triaxiality and the hydrostatic pressure do not vary uniformly, which is a result of too few elements in the Z direction. It must be emphasized that the computational time and effort increase significantly with increasing the element in the Z direction.

Figure 10 shows the total void volume fraction (f) at point A, and it demonstrates that the growth of f decreases with a decrease in specimen width. As mentioned previously, the change in strain path as well as decrease in stress triaxiality are the main reasons for the decreased void growth.

The ductility of the sheet is measured in terms of the fracture strain $\left(\epsilon_c = \ln\left(\frac{t_0}{t_f}\right)\right)$, where t_0 and t_f are the initial and final thickness of sheet in the middle section of specimen, respectively. Figure 11 shows the fracture strain of specimen with various widths and it is observed that the fracture strain decreases with an increase of width. The decrease in fracture strain can be explained by considering the variation in void volume fraction of specimens with various widths. Void volume fraction decreases with decreasing width and this causes an increase in ductility. It is to be noted that fracture does not occur for the sheet with a width of 2.5 mm.



(a)



(b)

Figure 9. Effect of width on (a) hydrostatic pressure and (b) stress triaxiality at point A.

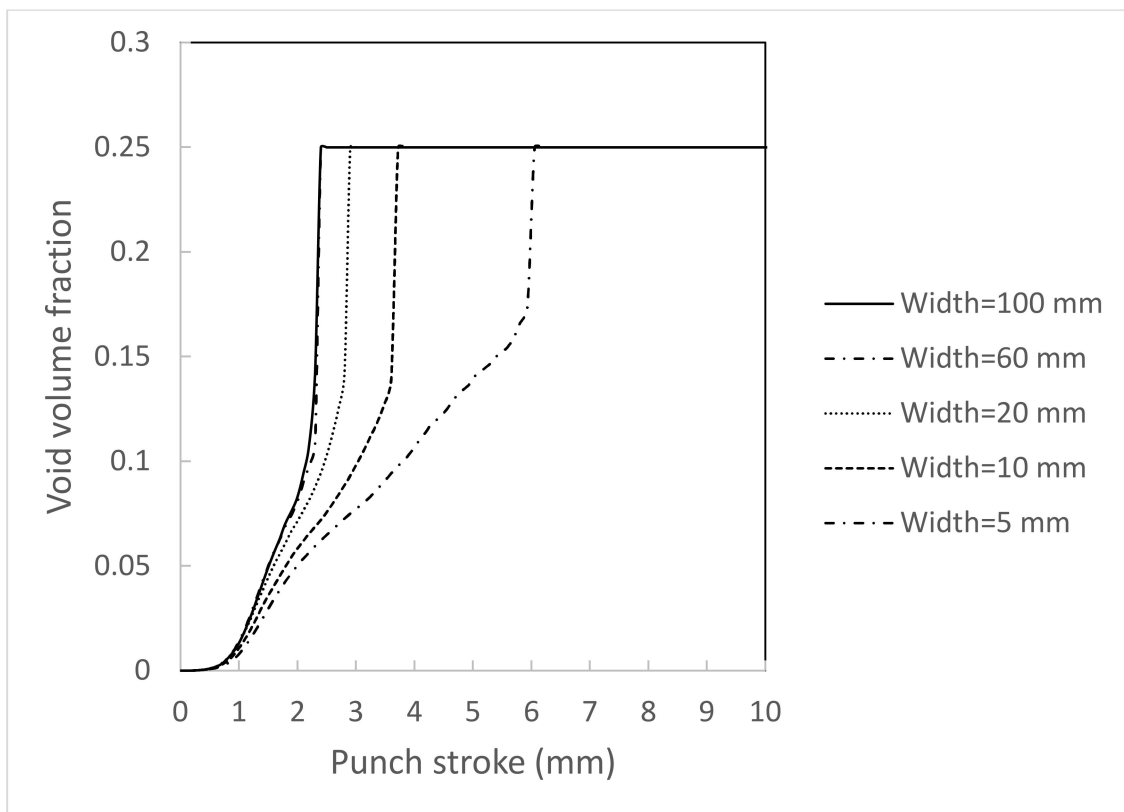


Figure 10. Void volume fractions at point A in metal sheets with various widths.

4.2. Effect of Pressure on Bendability

The effect of superimposed hydrostatic pressure ($p = -\alpha\sigma_y$) on bendability in sheet metals under in-plane plane strain condition using ABAQUS is studied in [10]. The GTN model is used in this study and shows that void growth decreases with increased pressure while void nucleation remains constant as a result of the constant nucleation strain in the GTN model. As observed, ductility increases with increased pressure. In this study the effect of superimposed hydrostatic pressure on a 10 mm-wide sheet of constant thickness is examined using ABAQUS. The superimposed pressure is examined in two steps. First the pressure is applied to all surfaces from zero to $p = -\alpha\sigma_y$, then the punch is advanced through the middle section of the sheet keeping the pressure constant. Figure 12 shows the volumetric strain at point A in the sheet for different superimposed pressures and clearly the strain path changes with pressure. It needs to be emphasized that the effect of pressure on surfaces perpendicular to the Z direction is considered contrary to the simulation in [10], where a 2D plain strain element was considered. The changes in the volumetric strain lead to a decrease in the tendency for fracture from void growth, and this delays the fracture process. Fracture does not occur for $\alpha = 0.1$ and 0.2. The volumetric strain in these cases increases and then decreases as the sheet slides over the mandrel, similar to what happened for the 2.5 mm sheet shown in Figure 8.

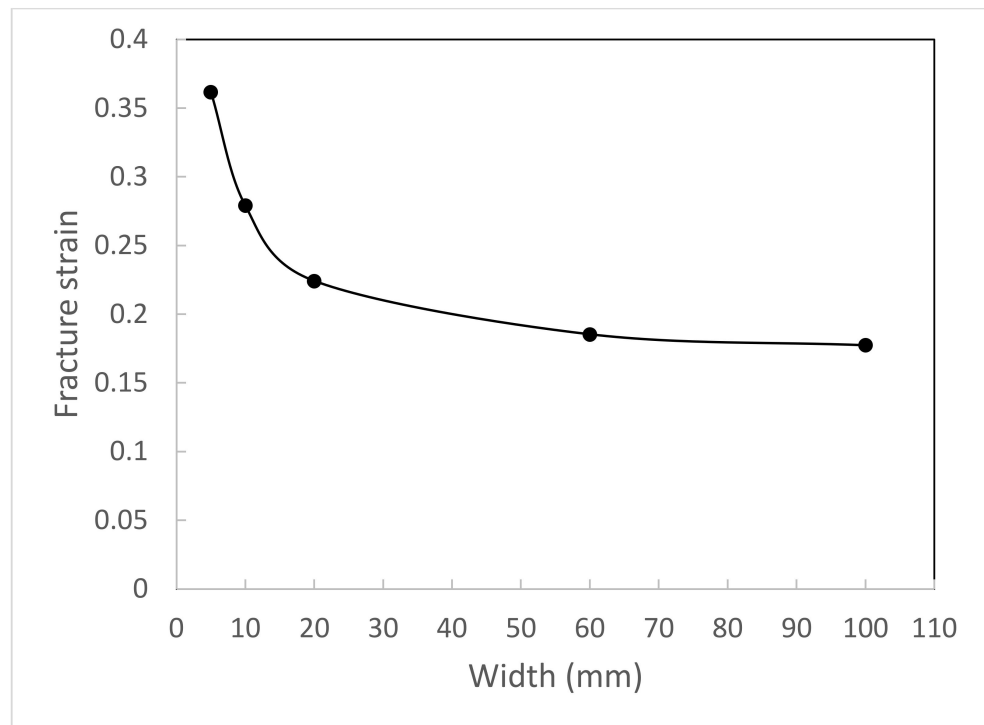


Figure 11. Fracture bending strain in metal sheets with various widths.

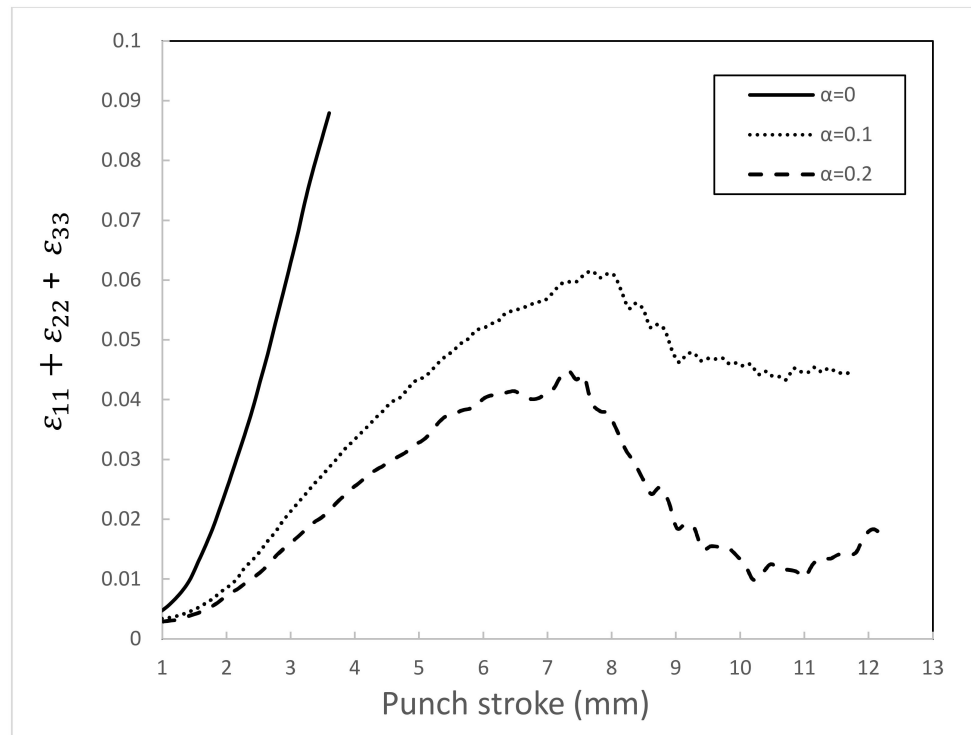
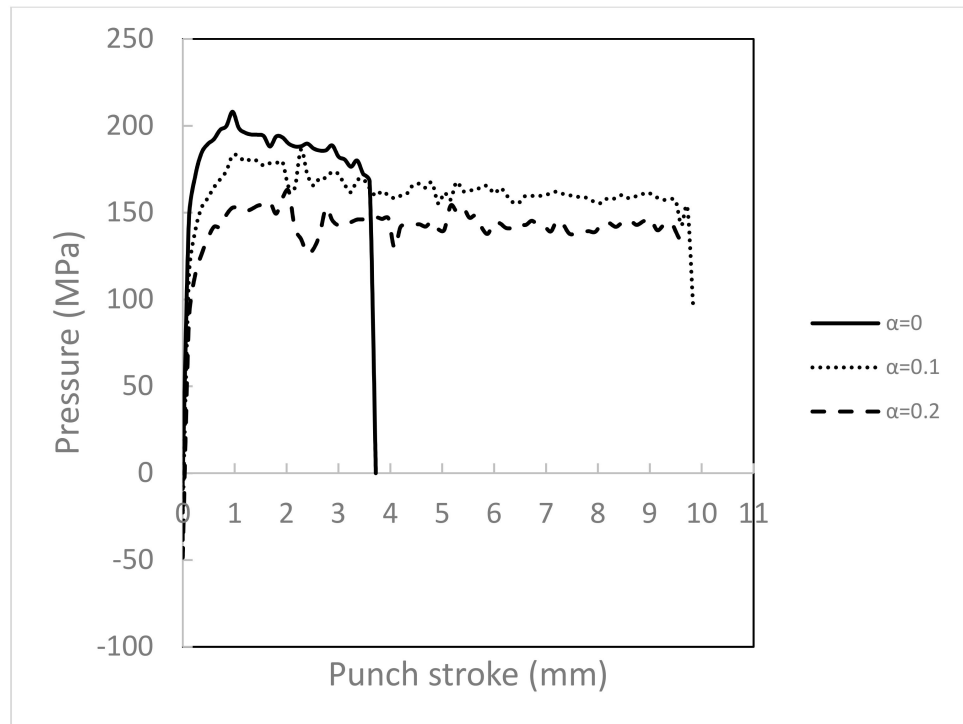
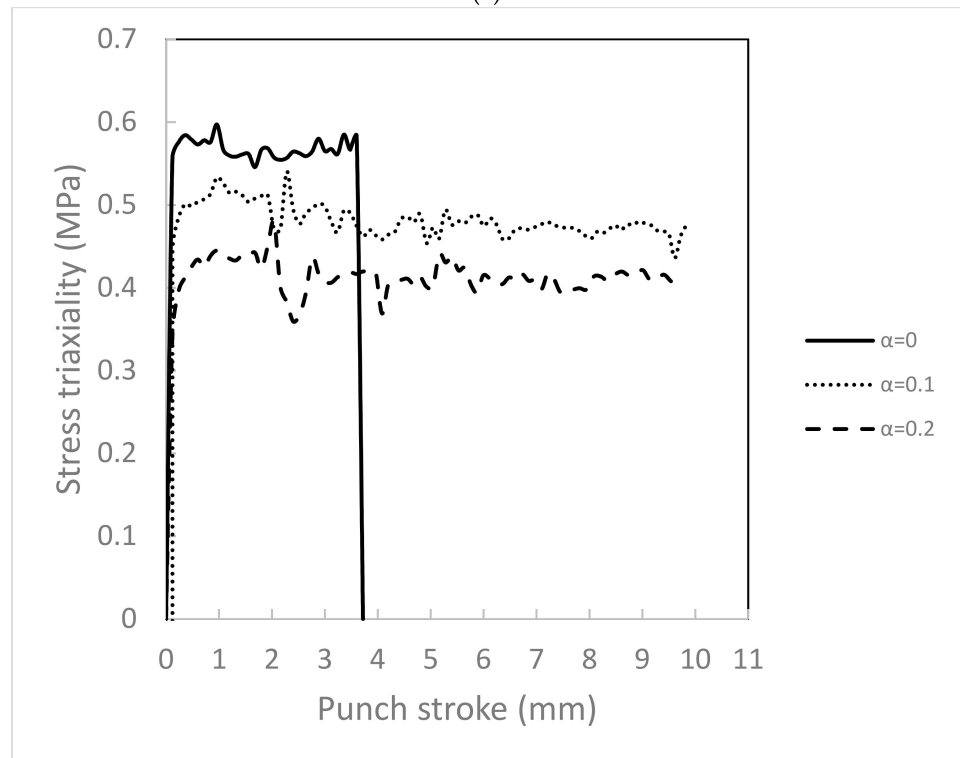


Figure 12. Volumetric strain in metal sheet with 10 mm width under various pressures.

Figure 13 presents the hydrostatic pressure and stress triaxiality at point A (see Figure 2), where fracture initiates as a function of punch stroke under various pressures. It is found that stress-triaxiality and hydrostatic pressure decrease with increasing the pressure and this helps delay void growth following Equation (6).



(a)



(b)

Figure 13. Effect of superimposed hydrostatic pressure on (a) hydrostatic pressure and (b) stress triaxiality at point A for a sheet with width = 10 mm.

The fracture strains calculated for different width sheets under various pressures are shown in Figure 14. Fracture does not occur under superimposed pressure in most cases. However, for those cases where fracture does occur the results show that the fracture strain increases with decreasing width as well as increasing pressure. This numerical study shows

that the ductility enhancement through decreasing specimen width is somewhat similar to increasing the pressure. It has a similar effect up to pressure of $\alpha = 0.2$.

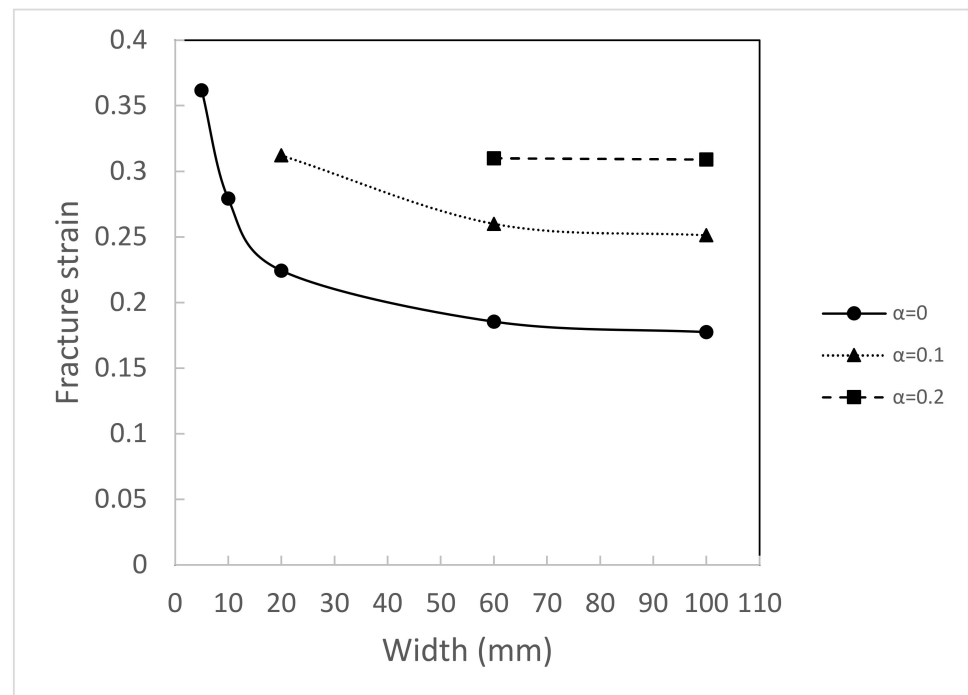


Figure 14. Fracture bending strain in metal sheets with different widths under various pressures.

5. Conclusions

In this study a FE analysis of the three-point bend test for sheet metal with various width/thickness ratios is carried out. It is found that a lower width/thickness ratio improves bendability significantly as the stress triaxiality decreases in the sheet, leading to lower fracture strain. The volumetric strain and stress triaxiality decrease with decrease in width/thickness ratio, and this delays void growth and coalescence. Thus, the fracture strain increases with decreasing width/thickness ratio. Moreover, the effect of superimposed hydrostatic pressure of sheet metals on fracture strain is studied. The hydrostatic pressure increases the fracture strain. It is observed numerically in this study that the effect of width/thickness ratio in increasing the fracture strain is similar to that which happens under applied pressure. Fracture does not happen in narrow sheets under superimposed pressure and the effect of pressure on fracture strain cannot be measured. On the contrary, the numerical results show that the effect of superimposed hydrostatic pressure on fracture strain can be measured by increasing the width/thickness ratio in sheets.

Author Contributions: Conceptualization, M.S., D.L. and P.W.; methodology, M.S. and P.W.; software, P.W.; validation, M.S., D.L. and P.W.; formal analysis, M.S., D.L. and P.W.; investigation, M.S., D.L. and P.W.; writing—original draft preparation, M.S., D.L., A.P. and P.W.; writing—review and editing, M.S., D.L., A.P. and P.W.; visualization, M.S., D.L., A.P. and P.W.; supervision, P.W.; project administration, M.S.; funding acquisition, P.W. All authors have read and agreed to the published version of the manuscript.

Funding: This research received no external funding.

Institutional Review Board Statement: Not applicable.

Informed Consent Statement: Not applicable.

Data Availability Statement: Not applicable.

Conflicts of Interest: The authors declare no conflict of interest.

References

1. Ragab, A.; Saleh, C.A. Evaluation of bendability of sheet metals using void coalescence models. *Mater. Sci. Eng. A* **2005**, *395*, 102–109. [[CrossRef](#)]
2. Jin, Y.; Murata, M. Influence of pitch and cross-sectional ratio of strip of sheet metal on incremental in-plane bending. *J. Mater. Process. Technol.* **2004**, *155*, 1810–1814. [[CrossRef](#)]
3. Lloyd, D.J.; Gallerneault, M.; Wagstaff, R.B. The deformation of clad aluminum sheet produced by direct chill casting. *Metall. Mater. Trans. A* **2010**, *41*, 2093–2103. [[CrossRef](#)]
4. Shi, Y.; Zhao, P.Z.; Jin, H.; Wu, P.D.; Lloyd, D.J. Analysis of surface roughening in AA6111 automotive sheet under pure bending. *Metall. Mater. Trans. A* **2016**, *47*, 949–960. [[CrossRef](#)]
5. Lloyd, D.J.; Evans, D.; Pelow, C.; Nolan, P. Bending in aluminium alloys AA 6111 and AA 5754 using the cantilever bend test. *Mater. Sci. Technol.* **2002**, *18*, 621–628. [[CrossRef](#)]
6. Sarkar, J.; Kutty, T.R.G.; Conlon, K.T.; Wilkinson, D.S.; Embury, J.D.; Lloyd, D.J. Tensile and bending properties of AA5754 aluminum alloys. *Mater. Sci. Eng. A* **2001**, *316*, 52–59. [[CrossRef](#)]
7. Sarkar, J.; Kutty, T.R.G.; Wilkinson, D.S.; Embury, J.D.; Lloyd, D.J. Tensile properties and bendability of T4 treated AA6111 aluminum alloys. *Mater. Sci. Eng. A* **2004**, *369*, 258–266. [[CrossRef](#)]
8. Hou, P.; Zhao, H.; Ma, Z.; Zhang, S.; Li, J.; Dong, X.; Sun, Y.; Zhu, Z. Influence of punch radius on elastic modulus of three-point bending tests. *Adv. Mech. Eng.* **2016**, *8*, 1–8. [[CrossRef](#)]
9. Datsko, J.; Yang, C.T. Correlation of bendability of materials with their tensile properties. *J. Manuf. Sci. Eng.* **1960**, *82*, 309–313. [[CrossRef](#)]
10. Shahzamanian, M.M.; Wu, D.J.L.P.D.; Xu, Z. Study of influence of superimposed hydrostatic pressure on bendability of sheet metals. *Eur. J. Mech. A/Solids* **2021**, *85*, 104132. [[CrossRef](#)]
11. Shahzamanian, M.M.; Lloyd, D.; Wu, P.D. Enhanced bendability in sheet metal produced by cladding a ductile layer. *Mater. Today Commun.* **2020**, *23*, 100952. [[CrossRef](#)]
12. Kao, A.S.; Kuhn, H.A.; Richmond, O.; Spitzig, W.A. Workability of 1045 spheroidized steel under superimposed hydrostatic pressure. *Metall. Trans. A* **1989**, *20*, 1735–1741.
13. Kõrgesaar, M. The effect of low stress triaxialities and deformation paths on ductile fracture simulations of large shell structures. *Mar. Struct.* **2019**, *63*, 45–64. [[CrossRef](#)]
14. Wierzbicki, T.; Bao, Y.; Lee, Y.W.; Bai, Y. Calibration and evaluation of seven fracture models. *Int. J. Mech. Sci.* **2005**, *47*, 719–743. [[CrossRef](#)]
15. Kao, A.S.; Kuhn, H.A.; Richmond, O.; Spitzig, W.A. Tensile fracture and fractographic analysis of 1045 spheroidized steel under hydrostatic pressure. *J. Mater. Res.* **1990**, *5*, 83–91. [[CrossRef](#)]
16. Weinrich, P.; French, I. The influence of hydrostatic pressure on the fracture mechanisms of sheet tensile specimens of copper and brass. *Acta Metall.* **1976**, *24*, 317–322. [[CrossRef](#)]
17. Ashby, M.F.; Embury, J.D.; Cooksley, S.H.; Teirlinck, D. Fracture maps with pressure as a variable. *Scr. Metall.* **1985**, *19*, 385–390. [[CrossRef](#)]
18. French, I.E.; Weinrich, P.F. The influence of hydrostatic pressure on the tensile deformation and fracture of copper. *Metall. Trans. A* **1975**, *6*, 785. [[CrossRef](#)]
19. French, I.; Weinrich, P.; Weaver, C. Tensile fracture of free machining brass as a function of hydrostatic pressure. *Acta Metall.* **1973**, *21*, 1045–1049. [[CrossRef](#)]
20. Brownrigg, A.; Spitzig, W.A.; Richmond, O.; Teirlinck, D. The influence of hydrostatic pressure on the flow stress and ductility of a spheroidized 1045 steel. *Acta Metall.* **1983**, *31*, 1141–1150. [[CrossRef](#)]
21. Partovi, A.; Shahzamanian, M.M.; Wu, P.D. Study of Influence of Superimposed Hydrostatic Pressure on Ductility in Ring Compression Test. *J. Mater. Eng. Perform.* **2020**, *29*, 6581–6590. [[CrossRef](#)]
22. Tvergaard, V.; Needleman, A. Analysis of the cup-cone fracture in a round tensile bar. *Acta Metall.* **1984**, *32*, 157–169. [[CrossRef](#)]
23. Tvergaard, V. Influence of voids on shear band instabilities under plane strain conditions. *Int. J. Fract.* **1981**, *17*, 389–407. [[CrossRef](#)]
24. Tvergaard, V. On localization in ductile materials containing spherical voids. *Int. J. Fract.* **1982**, *18*, 237–252.
25. Gurson, A.L. Continuum theory of ductile rupture by void nucleation and growth: Part I—Yield criteria and flow rules for porous ductile media. *J. Eng. Mater. Technol.* **1977**, *99*, 2–15. [[CrossRef](#)]
26. Shahzamanian, M.M.; Partovi, A.; Wu, P.D. Study of Pre-strain Effect on Bendability in Three-Point Bending Test. In *Fracture Fatigue and Wear*; Springer: Berlin/Heidelberg, Germany, 2020; pp. 261–268.
27. Schowtjak, A.; Kusche, C.F.; Meya, R.; Korte-Kerzel, S.; Al-Samman, T.; Tekkaya, A.E.; Clausmeyer, T. Prediction of void evolution in sheet bending based on statistically representative microstructural data for the Gurson-Tvergaard-Needleman model. *arXiv* **2020**, arXiv:2006.15973.
28. Andersen, R.G.; Londono, J.G.; Woelke, P.B.; Nielsen, K.L. Fundamental differences between plane strain bending and far-field plane strain tension in ductile plate failure. *J. Mech. Phys. Solids* **2020**, *141*, 103960. [[CrossRef](#)]
29. Achineethongkham, K.; Uthaisangsuk, V. Analysis of forming limit behaviour of high strength steels under non-linear strain paths using a micromechanics damage modelling. *Int. J. Mech. Sci.* **2020**, *183*, 105828. [[CrossRef](#)]

30. Shahzamanian, M.M. Anisotropic Gurson-Tvergaard-Needleman plasticity and damage model for finite element analysis of elastic–plastic problems. *Int. J. Numer. Methods Eng.* **2018**, *115*, 1527–1551. [[CrossRef](#)]
31. Malcher, L.; Pires, F.M.A.; de Sá, J.M.A.C. An extended GTN model for ductile fracture under high and low stress triaxiality. *Int. J. Plast.* **2014**, *54*, 193–228. [[CrossRef](#)]
32. Bergo, S.; Morin, D.; Hopperstad, O.S. Numerical implementation of a non-local GTN model for explicit FE simulation of ductile damage and fracture. *Int. J. Solids Struct.* **2021**, *219–220*, 134–150. [[CrossRef](#)]
33. He, Z.; Zhu, H.; Hu, Y. An improved shear modified GTN model for ductile fracture of aluminium alloys under different stress states and its parameters identification. *Int. J. Mech. Sci.* **2021**, *192*, 106081. [[CrossRef](#)]
34. Li, X.; Chen, Z.; Dong, C. Size effect on the damage evolution of a modified GTN model under high/low stress triaxiality in meso-scaled plastic deformation. *Mater. Today Commun.* **2021**, *26*, 101782. [[CrossRef](#)]
35. Chen, D.; Li, Y.; Yang, X.; Jiang, W.; Guan, L. Efficient parameters identification of a modified GTN model of ductile fracture using machine learning. *Eng. Fract. Mech.* **2021**, *245*, 107535. [[CrossRef](#)]
36. Yildiz, R.A.; Yilmaz, S. Influence of heat treatments on the formability of the 6061 Al alloy sheets: Experiments and GTN damage model. *Int. J. Adv. Manuf. Technol.* **2021**, *113*, 2277–2299. [[CrossRef](#)]
37. ABAQUS Inc. *A.M.V.*; Dassault Systèmes: Providence, RI, USA, 2014.
38. Chu, C.; Needleman, A. Void nucleation effects in biaxially stretched sheets. *J. Eng. Mater. Technol.* **1980**, *102*, 249–256. [[CrossRef](#)]
39. Wu, P.D.; Chen, X.X.; Lloyd, D.J.; Embury, J.D. Effects of superimposed hydrostatic pressure on fracture in sheet metals under tension. *Int. J. Mech. Sci.* **2010**, *52*, 236–244. [[CrossRef](#)]
40. Chen, X.X.; Wu, P.D.; Lloyd, D.J.; Embury, J.D.; Huang, Y. Enhanced ductility in sheet metals produced by cladding a ductile layer. *J. Appl. Mech.* **2010**, *77*, 41015. [[CrossRef](#)]
41. Peng, J.; Wu, P.D.; Huang, Y.; Chen, X.X.; Lloyd, D.J.; Embury, J.D.; Neale, K.W. Effects of superimposed hydrostatic pressure on fracture in round bars under tension. *Int. J. Solids Struct.* **2009**, *46*, 3741–3749. [[CrossRef](#)]
42. Chen, X.X.; Wu, P.D.; Embury, J.D.; Huang, Y. Enhanced ductility in round tensile bars produced by cladding a ductile ring. *Model. Simul. Mater. Sci. Eng.* **2010**, *18*, 25005. [[CrossRef](#)]